Journal of Power Sources 195 (2010) 1583–1588

Contents lists available at ScienceDirect

Journal of Power Sources

journal homepage: www.elsevier.com/locate/jpowsour

Borohydride electrochemical oxidation on carbon-supported Pt-modified Au nanoparticles

Xiaoying Geng[a,b], Huamin Zhang[a,*], Yuanwei Ma[a,b], Hexiang Zhong[a]

[a] Lab of PEMFC Key Materials and Technologies, Dalian Institute of Chemical Physics, Chinese Academy of Sciences, Dalian 116023, China
[b] Graduate School of the Chinese Academy of Sciences, Beijing 100039, China

ARTICLE INFO

Article history:
Received 28 July 2009
Received in revised form
14 September 2009
Accepted 15 September 2009
Available online 23 September 2009

Keywords:
Direct borohydride fuel cell (DBFC)
AuPt catalyst
Surface structure
Borohydride oxidation
Hydrogen evolution

ABSTRACT

The carbon-supported Pt-modified Au nanoparticles were prepared by two different chemical reduction processes, the simultaneous chemical reduction of Pt and Au on carbon process (A-AuPt/C) and the successive reduction of Au then Pt (B-AuPt/C) on carbon process. These two catalysts were investigated as the anode catalysts for a direct borohydride fuel cell (DBFC) and Au nanoparticles on carbon (Au/C) were also prepared for comparison. The DBFC with B-AuPt/C as the anode catalyst shows the best anode and fuel cell performance. The maximum power density with the B-AuPt/C catalyst is 112 mW cm^{-2} at 40 °C, compared to 97 mW cm^{-2} for A-AuPt/C and 65 mW cm^{-2} for Au/C. In addition, the DBFC with the B-AuPt/C catalyst shows the best fuel utilization with a maximum apparent number of electrons (N_{app}) equal to 6.4 in 1 M $NaBH_4$ and 7.2 in 0.5 M $NaBH_4$ as compared to the value of N_{app} of 8 for complete utilization of borohydride.

1. Introduction

The growing power consumption and the desire for more autonomy in portable and mobile electronic devices have spurred the development of more energy dense power sources. Borohydride has been widely investigated as a hydrogen storage material due to its high gravimetric hydrogen capacity, for example, $NaBH_4$ contains 10.6 wt.% hydrogen. Also, $NaBH_4$ is readily available, safe and easily transported. Recently, direct borohydride fuel cell (DBFC) has gained a lot of attention as a potential power source for portable application due to its theoretical high energy density and high cell voltage. The anode reaction of the DBFC is the direct oxidation of borohydride in alkaline medium:

$$BH_4^- + 8OH^- \rightarrow BO_2^- + 6H_2O + 8e^-, \quad E^0 = -1.24\,V \qquad (1)$$

Although hydrogen gas as the anode fuel can be obtained from the hydrolysis of borohydride (Eq. (2)), the direct anodic oxidation of borohydride provides a higher cell voltage compared with oxidizing molecular hydrogen.

$$BH_4^- + 2H_2O \rightarrow BO_2^- + 4H_2\uparrow \qquad (2)$$

However, before a practical DBFC can be realized in a fuel cell system, the challenge of finding an anode catalyst that can perform specific and efficient oxidation of the borohydride must be found. Many catalysts such as noble metals [1–13], transition metals [3,14], hydrogen storage alloys [15–18] and bimetallic catalysts [9,19,20] have been evaluated as anode catalysts for DBFC. The direct oxidation of borohydride involves eight electrons (8e) per molecule in principle (Eq. (1)), while in practice the 8e oxidation is only observed on very few electrodes [1,3,5,12,21–24], which usually demonstrate slow electrode kinetics and thus low current and power output [5,11,23]. On the other hand, some catalysts, such as Pt, Pd, Ni, and hydrogen storage alloys, are known to be highly active for borohydride oxidation, but these are also highly active toward the undesirable hydrogen hydrolysis reaction (Eq. (2)) [14,18].

Gold has been investigated as a catalyst for borohydride oxidation with almost no catalytic activity for borohydride hydrolysis [1,14]. But the catalytic activity of Au is low [14,15]. In view of the selectivity of the catalytic property of gold and the high catalytic activity of platinum towards borohydride oxidation, bimetallic AuPt nanoparticles of controllable structure were studied for a catalyst with enhanced the catalytic activity and conversion efficiency during the electro-oxidation of BH_4^-.

In our present work, the carbon-supported Pt-modified Au catalysts were prepared with two processes, the simultaneous chemical reduction process and the successive chemical reduction process, compared with the unmodified Au nanoparticles. The influence of reduction process on the surface structures of the catalysts, and the corresponding electro-catalytic activities and efficiencies towards borohydride oxidation were investigated. The electro-

* Corresponding author. Tel.: +86 411 84379072 fax: +86 411 84665057.
E-mail address: zhanghm@dicp.ac.cn (H. Zhang).

0378-7753/$ – see front matter © 2009 Elsevier B.V. All rights reserved.
doi:10.1016/j.jpowsour.2009.09.036

catalytic activities towards borohydride oxidation were evaluated by voltammetry and single cell test. The efficiency of the DBFC was expressed by the apparent number of electrons (N_{app}) [25], which was calculated by evaluating the hydrogen evolution rate at definite current density in the practical DBFC. Furthermore, the influence of borohydride concentration on the activity of the AuPt/C catalyst was also evaluated.

2. Experiment

2.1. Preparation of the catalysts

The carbon-supported Au (Au/C) catalyst was prepared according to the method reported in Ref. [26]. The 20 wt.% Au/C catalyst was prepared as follows: 4.62 ml of 0.033 mM $HAuCl_4$ solution was added into 800 ml of deionized (DI) water and stirred vigorously, followed by the addition of 10 ml aqueous solution containing 100 mg sodium citrate ($Na_3C_6H_5O_7{\cdot}2H_2O$). One minute later, 10 ml solution containing 30 mg $NaBH_4$ and 100 mg sodium citrate was added quickly. The mixture was stirred for 1 h, and then 120 mg Vulcan XC-72R carbon black (Cabot Corp., $S_{BET} = 250\ m^2\ g^{-1}$) was added. After stirring for 48 h and then standing for 24 h, the color of the solution turned from red to transparence, indicating that Au colloid particles were supported on the carbon particles. Finally, the catalyst was precipitated, washed with DI water and then dried in a vacuum oven at 80 °C.

The carbon-supported Pt-modified Au catalysts were prepared with two processes, the simultaneous chemical reduction process (A-AuPt/C) and the successive chemical reduction process (B-AuPt/C). As for the preparation of A-AuPt/C catalyst with metal loading as 20 wt.% and molar ratio of Pt and Au as 2:18, 4.16 ml of 0.033 mM $HAuCl_4$ and 1.03 ml of 0.015 mM H_2PtCl_6 were added into 800 ml of DI water simultaneously. And the following procedure was the same as that of Au/C. The procedure of preparing B-AuPt/C was similar to that of AuPt core-shell catalyst as reported in Ref. [26]: 10 ml solution containing 300 mg ascorbic acid ($C_6H_8O_6$) was added to 720 ml of the as-prepared Au colloid (containing 27 mg Au), followed by the addition of 70 ml of H_2PtCl_6 solution containing 3 mg Pt^{4+}. The mixture was stirred for 1 h, and 120 mg Vulcan XC-72R carbon black was added. After stirring for 48 h and then standing for 24 h, the catalyst was separated, washed, dried, and obtained the B-AuPt/C catalyst with 20% metal loading and the molar ratio of Pt and Au as 2:18. The procedure of the catalyst preparation was illustrated in Scheme 1.

2.2. Half-cell tests

An EG & G 263 potentiostat/galvanostat was used for the electrochemical measurements in a three-electrode test cell. The working electrode was a thin porous coating disk electrode with a diameter of 4 mm. The thin porous coating disk electrode design was described in our previous work [27]. About 2.5 mg catalyst was ultrasonically suspended in 1.0 ml isopropanol and 10 μl Nafion (5 wt.%) solution for about 30 min to obtain a well-dispersed catalyst ink, then 20 μl of the catalyst ink was spread onto the surface of a clean glass carbon electrode and dried at 120 °C. The counter electrode was a graphite plate (exposed area = 8.0 cm^2) and a Hg/HgO (2 M NaOH) electrode was used as reference. The potential of the Hg/HgO electrode was −0.139 V with respect to a saturated calomel electrode. And all the potentials were expressed towards the normal hydrogen electrode (NHE). The surface electrochemistry of the catalyst was studied by cyclic voltammetry (CV) at 100 mV s^{-1} in 2 M NaOH. The electrochemical behavior of borohydride on the catalyst was studied on a rotating disc electrode (RDE) in 0.01 M $NaBH_4$ + 2 M NaOH solution at a scan rate of 5 mV s^{-1} and a rotating speed of 800 rpm. The cell was maintained at room temperature under nitrogen atmosphere to eliminate trace of dissolved oxygen.

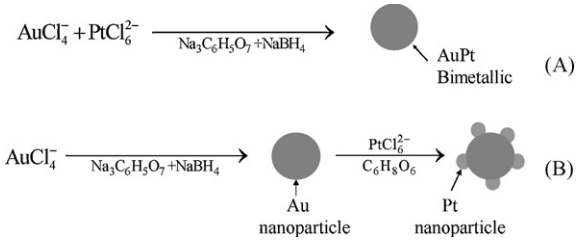

Scheme 1. Procedure to design the AuPt nanoparticles: (A) A-AuPt/C, (B) B-AuPt/C.

2.3. Single cell tests

The core part of the DBFC consisted basically of two electrodes (anode and cathode) separated by a Na^+ form Nafion 212 membrane (Du Pont). Single-channel serpentine flow field was used at both anode and cathode side. Details of the testing system of the single fuel cell were described in our previous paper [27].

The anode of the DBFC was prepared as follows: First, the prepared catalyst (113 mg) was mixed with 250 mg of 5% Nafion solution and 8 ml ethanol, and ultrasonicated to form ink-like slurry. And then an appropriate amount of the slurry was cast onto the carbon paper (Toray) and dried to obtain the anode electrode with metal loading of 1.0 mg cm^{-2}. The cathode adopted the commercial 46 wt.% Pt/C (TKK Corp.) with Pt loading of 0.5 mg cm^{-2}.

For single cell test, the effective geometrical area of the electrode was 5 cm^2 and an alkali $NaBH_4$ borohydride solution containing x mol $NaBH_4$ (x = 0.2, 0.5, 1.0, 1.5) and 2 M NaOH was fed to the anode inlet at a flow rate of 0.5 ml min^{-1} by a qualitative fuel pump. Oxygen gas (0.2 Mpa) was fed to the cathode inlet at a flow rate of 0.1 l min^{-1} without humidification. The amount of hydrogen gas produced during operation was measured using a flow meter and the volume was converted into the value at the standard temperature and pressure.

2.4. Physical characterizations of the catalysts

A Philips CM-1 Power X-ray diffractometer was employed using Cu Kα source (k = 1.54056 Å) to obtain XRD spectra of the catalysts. The tube current and voltage were 100 mA and 40 kV, respectively. The angle extended from 20° to 90° and varied at a rate of

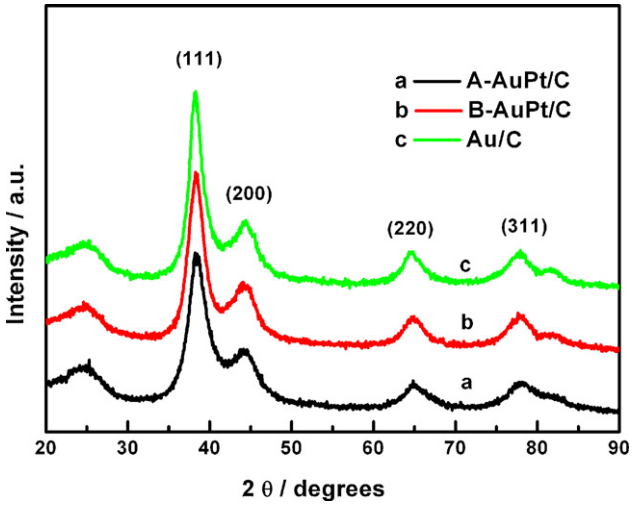

Fig. 1. XRD patterns of different catalysts.

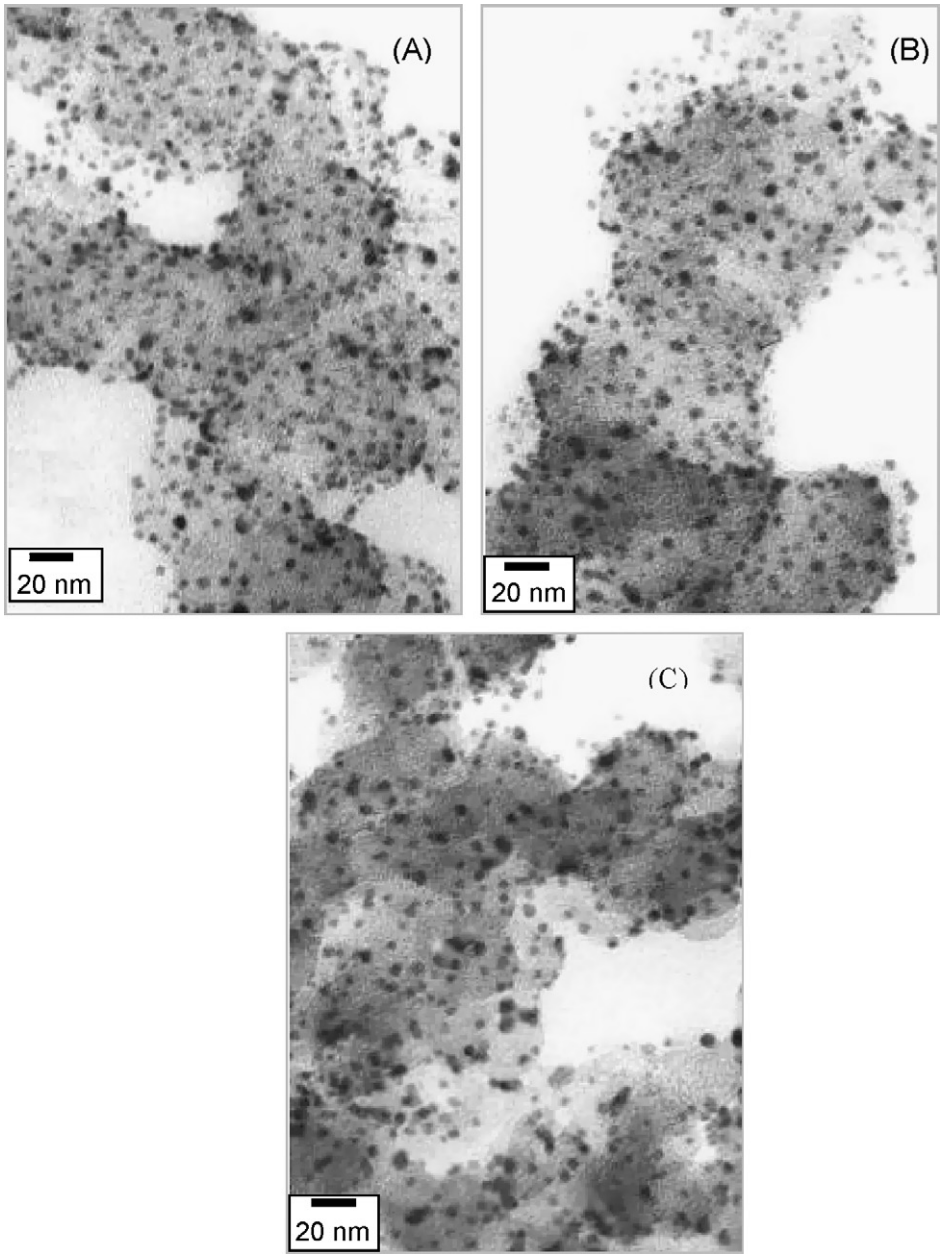

Fig. 2. TEM images of the catalysts: (A) TEM image of Au/C, (B) TEM image of A-AuPt/C, (C) TEM image of B-AuPt/C.

$10^{\circ}\ min^{-1}$. Scherrer's formula was employed to obtain the average particle size. Inductively coupled plasma (ICP) analyses of the Au/C, A-AuPt/C and B-AuPt/C catalysts were conducted with Optima 2000DV to determine bulk contents of the metals.

TEM measurements on JEOL JEM-2011 were carried out to evaluate the morphologies and particle size distributions of the catalysts. For each sample, the catalyst powder was ultrasonically suspended in ethanol and a drop of the suspension was applied to a copper grid and the ethanol was allowed to evaporate. At least 200 particles were calculated to obtain the integrated information about the overall distribution of the catalyst.

3. Results and discussion

3.1. Physical characterizations

Fig. 1 presents the X-ray diffraction patterns of the Au/C, A-AuPt/C, B-AuPt/C catalyst. As it is shown in the figure, both of the nanocomposites exhibit only characteristic diffraction peaks of the fcc gold [19]. No diffraction peaks, which would be attributed to platinum, appear in the XRD patterns. The average crystallite sizes for the Au/C, A-AuPt/C, B-AuPt/C catalysts, calculated by Scherrer's formula, are 4.0, 3.8 and 3.9 nm, respectively, which are close to those obtained by TEM as shown in Fig. 2. Fig. 2A shows the image of the highly dispersed Au nanoparticles on the carbon support. The mean particle diameter of the Au nanoparticles is 4.3 nm. Fig. 2B and C shows the TEM images of A-AuPt/C and B-AuPt/C, respectively. In the Pt-modified Au nanoparticles on carbon support, the similar high dispersion as Au/C is obtained and the mean particle diameters of A-AuPt/C and B-AuPt/C are 4.2 and 4.5 nm, respectively. ICP was conducted to determine the bulk metal content in the Au/C and AuPt/C catalysts. The results show that the contents of Au and/or Pt in all the catalysts are very close to their nominal values.

Surface structure of electro-catalyst has a great effect on the catalytic reaction. As a surface sensitive technique, cyclic voltammetry was performed in solution of 2 M NaOH to obtain the surface com-

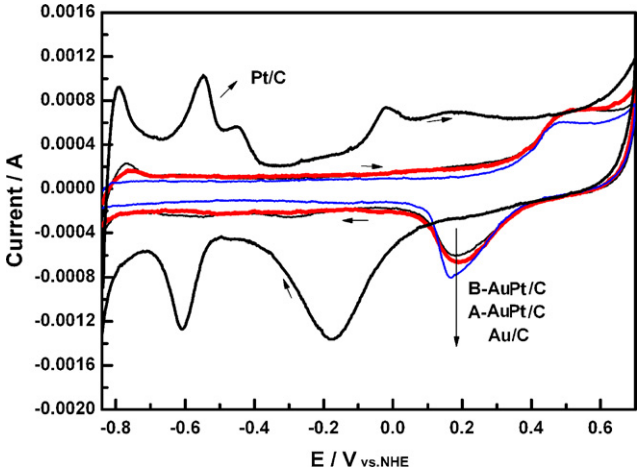

Fig. 3. Cyclic voltammograms on different catalysts in 2 M NaOH. Scan rate: 100 mV s^{-1}.

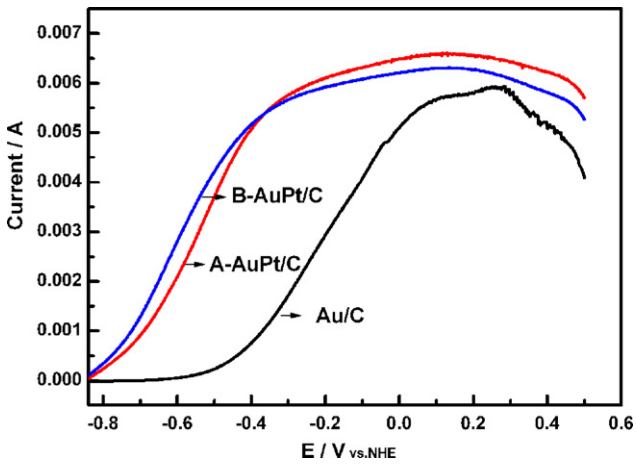

Fig. 4. Voltammograms of BH_4^- oxidation on different catalysts (positive-going scan). Scan rate: 5 mV s^{-1}; rotating speed: 800 rpm; $NaBH_4$ concentration: 0.01 M $NaBH_4$ in 2 M NaOH.

position and characteristic of the catalysts. Fig. 3 presents potential cycle voltammograms recorded in deaerated 2 M NaOH solution at the AuPt/C electrodes and, for comparison, at Au/C and Pt/C electrodes. The cyclic voltammogram on Au/C catalyst displays a typical voltammetric response of Au surface in alkaline condition [28], characterized by Au-oxide formation at 0.5 V in the positive scan and the Au-oxide reduction peak at 0.2 V in the negative scan. And the characteristic features of Au surface electrochemistry are clearly observed both at the A-PtAu/C and B-AuPt/C electrodes. Also, the hydrogen adsorption/desorption peaks and Pt oxide formation/stripping wave that characterize Pt are readily seen in both A-PtAu/C and B-AuPt/C electrodes, in the potential region of −0.84 to −0.4 V, at potentials higher than −0.40 V and in the potential range of 0 to −0.4 V, respectively. However, the intensity of the peak current at −0.74 V with respect to hydrogen reaction on Pt, and the peak at 0.2 V with respect to oxide stripping on Au, are different. This phenomenon indicates that on the surface of A-AuPt/C and B-AuPt/C catalysts, the amounts of exposed Au sites and exposed Pt sites are different, which may be caused by the different preparation processes. As for the A-AuPt/C catalyst, the Pt and Au precursors were mixed first and then reduced by $NaBH_4$. While for the B-AuPt/C catalyst, the Au colloid was prepared first, then H_2PtCl_6 was added, and ascorbic acid was carefully chosen as the reducing agent because it had been known that ascorbic acid acted only as a growth agent without forming a new nucleus [29]. Thus the Pt nanoparticles would grow on the surface of Au nanoparticles, and some Au exposed sites were covered with Pt. From the area of the Au-oxide reduction wave from 0.4 to 0.05 V, the coverage of Pt on the surface of Au can be calculated [33]. And then using the atomic radii and FCC crystal lattice parameters of Au and Pt, one can translate the ratio of their electroactive surface areas into the ratio of atomic compositions (electroactive) [34]. And it is found that the ratio of Au and Pt is 6.4:1 for B-AuPt/C and 13.8:1 for A-AuPt/C. This value of Au and Pt for B-AuPt/C is much lower than that for A-AuPt/C, indicating an enrichment of the surface with Pt for B-AuPt/C.

3.2. Borohydride electro-oxidation on the catalysts

Linear sweep voltammetry (LSV) of the glassy carbon electrode with different catalysts in the solution of 0.01 M NaBH4/2 M NaOH was tested at a scan rate of 5 mV s^{-1} and a rotating speed of 800 rpm to evaluate the behavior of borohydride electro-oxidation in the half-cell test. Fig. 4 shows the LSV of the A-AuPt/C and B-AuPt/C catalysts compared with that of the Au/C catalyst from −0.84 to 0.5 V at room temperature. The onset potential for BH_4^- oxidation wave is more negative than that of Au/C catalyst, indicating the Pt-modified Au catalysts are more active oxidation catalysts.

In order to further investigate the electro-oxidation behaviors on the Au catalyst and the Pt-modified Au catalysts, the single cell tests were carried out for the three anode catalysts for DBFC. Fig. 5 shows the performances of the single cells with different catalysts and 1 M $NaBH_4$/2 M NaOH at 40 °C. The best polarization performance of the DBFC is obtained on the B-AuPt/C catalyst, e.g., 0.573 V at 180 mA cm^{-2}, followed by the A-AuPt/C catalyst showing 0.516 V at 180 mA cm^{-2}. Under identical condition the Au/C anode catalyst yields only 0.363 V, apparently confirming the results in the linear sweep voltammetry. And the maximum power densities of the DBFC employing B-AuPt/C, A-AuPt/C and Au/C are 112, 97 and 65 mW cm^{-2}, respectively.

3.3. Hydrogen evolution

Hydrogen evolution usually occurs during the operation of the DBFC, which not only reduces coulombic efficiency but also causes other problems such as safety problems of the fuel cell system [13–15,18]. Hydrogen evolution behaviors based on the relation of hydrogen evolution rate and the operation current density of the DBFC on the Au-based catalysts are reported in Figs. 6 and 7. The

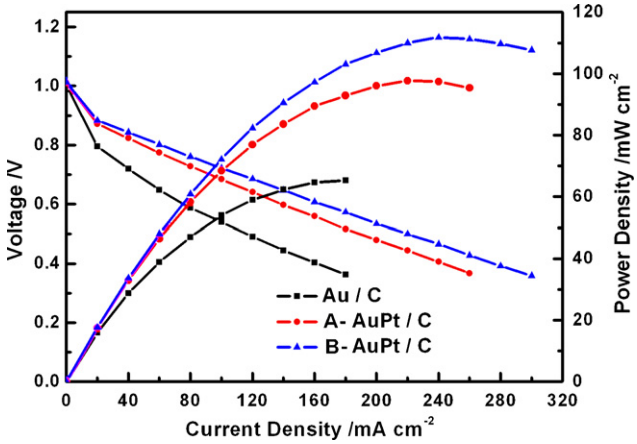

Fig. 5. Cell polarization curves of the DBFC using different anode catalysts at 40 °C. Anode catalyst loading: 1 mg metal cm^{-2}, 0.5 ml min^{-1} 1 M $NaBH_4$ in 2 M NaOH. Cathode catalyst loading: 0.5 mg Pt cm^{-2}, dry O_2 at 0.1 l min^{-1} (2 atm).

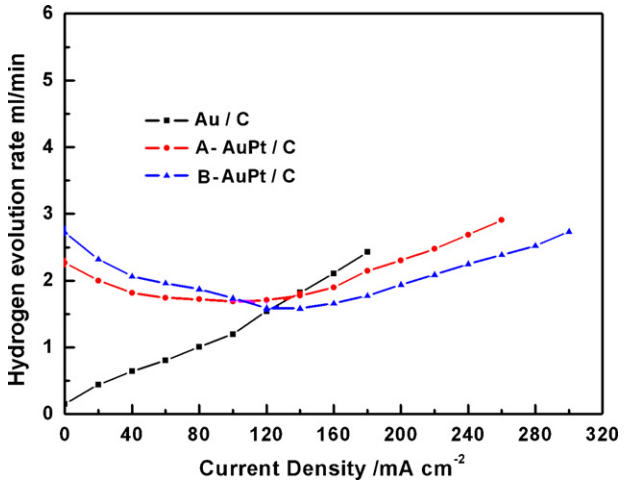

Fig. 6. Hydrogen evolution behaviors of the DBFC using different anode catalysts at 40 °C. Anode catalyst loading: 1 mg metal cm^{-2}, 0.5 ml min^{-1} 1 M $NaBH_4$ in 2 M NaOH. Cathode catalyst loading: 0.5 mg Pt cm^{-2}, dry O_2 at 0.1 l min^{-1} (2 atm).

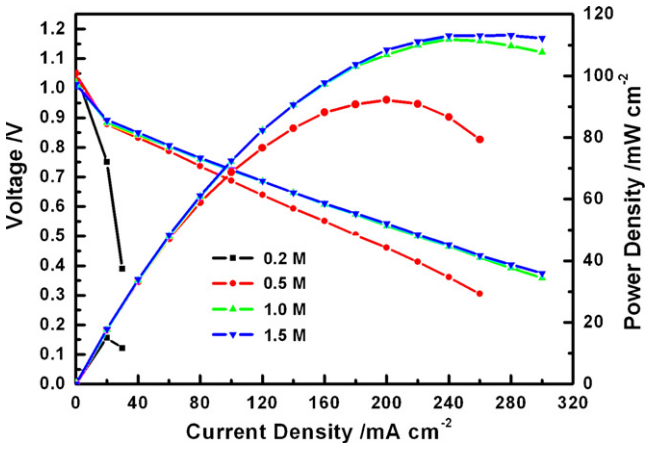

Fig. 8. Cell polarization curves of the DBFC using B-AuPt/C anode catalyst in different concentration of borohydride at 40 °C. Anode catalyst loading: 1 mg metal cm^{-2}, 0.5 ml min^{-1} × M $NaBH_4$ in 2 M NaOH. Cathode catalyst loading: 0.5 mg Pt cm^{-2}, dry O_2 at 0.1 l min^{-1} (2 atm).

utilization for borohydride is expressed by N_{app}, which represents the number of electrons released to the external circuit by each BH_4^- ion in the practical DBFC. N_{app} is calculated from recording the hydrogen evolution rate at definite current density of the DBFC and a N_{app}-value of 8 indicates that no hydrogen spills over from the anode of the DBFC. Note that N_{app} only appears to describe the fuel utilization in the DBFC, and is different from the number of electrons in reaction formulas.

Gold is an effective catalyst for BH_4^- oxidation but not for BH_4^- hydrolysis and many researchers found that the number of electrons transferred during the oxidation of BH_4^- in voltammetry experiments at Au electrodes was approximate to 8 [5,21,22,24,30]. The voltammetry experiments were often carried out at bulk Au electrode in relative low borohydride concentration in the half-cell test. In this paper, hydrogen evolution rate was evaluated on a practical DBFC using nano-Au as the anode catalyst, as shown in Fig. 6. It can be seen that the hydrogen evolution rate on the Au/C electrode is influenced by the discharge current density. At low current density, the hydrogen evolution rate is very low, but the hydrogen evolution rate increases with the increasing current density in the testing range and the N_{app} calculated is about 6 for Au/C catalyst as shown in Fig. 7, which is lower comparing with the reported results [21,22,30]. It may be caused by the hydrolysis of borohydride at the relatively high BH_4^- concentration or the particle size effect of the nano-Au particles. For A-AuPt/C and B-AuPt/C catalyst, the hydrogen generation rate at current lower than 120 mA cm^{-2} is higher than that on the Au/C catalyst, because Pt is a very active catalyst for BH_4^- hydrolysis. But with the current density increasing, the hydrogen generation rates on the Pt-modified catalysts are lower than that on Au/C catalyst, which may be caused by the fact that the hydrogen produced by hydrolysis of borohydride was further oxidized on the Pt nanoparticles [31]. Thus the N_{app}s calculated for the A-AuPt/C and B-AuPt/C catalyst are higher than on Au/C catalyst.

In addition, the maximum N_{app} value on the B-AuPt/C catalyst is 6.4, higher than 6.2 on the A-AuPt/C catalyst as shown in Fig. 7.

The behavior of borohydride oxidation on the catalyst surface is influenced by the borohydride concentration [32]. Fig. 8 shows the polarization curves and power densities of the DBFC using B-AuPt/C anode catalyst as a function of borohydride concentration between 0.2 and 1.5 M. Fig. 9 and Table 1 show the N_{app} values calculated at different borohydride concentrations. With the $NaBH_4$ concentration increasing from 0.2 to 1.5 M, the maximum power density of the DBFC increases but the maximum N_{app} value decreases consis-

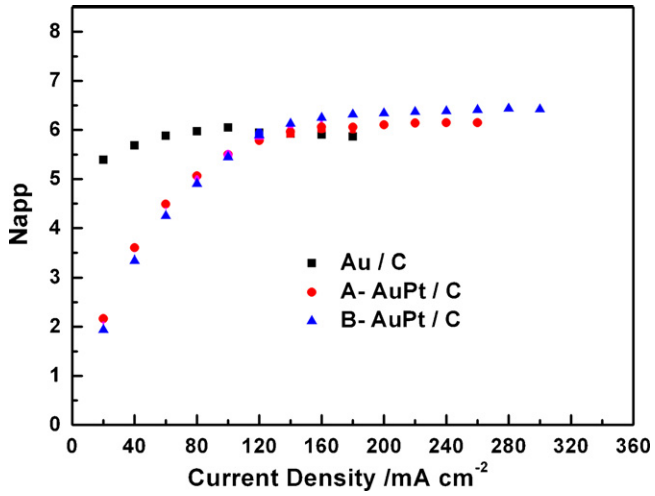

Fig. 7. N_{app} values of the DBFC using different anode catalysts at 40 °C. Anode catalyst loading: 1 mg metal cm^{-2}, 0.5 ml min^{-1} 1 M $NaBH_4$ in 2 M NaOH. Cathode catalyst loading: 0.5 mg Pt cm^{-2}, dry O_2 at 0.1 l min^{-1} (2 atm).

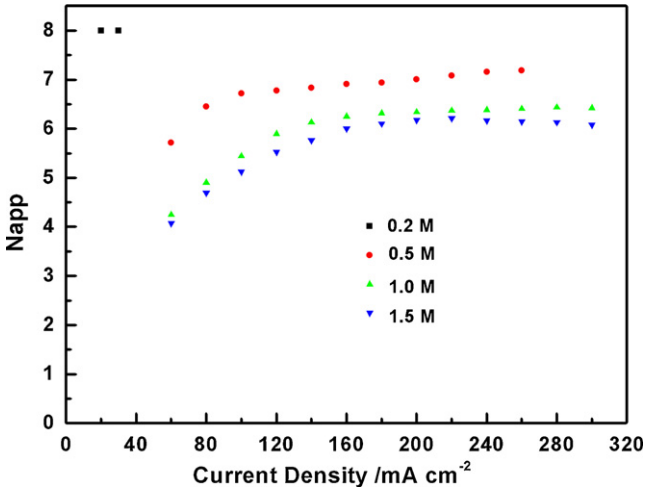

Fig. 9. N_{app} values of the DBFC using B-AuPt/C anode catalyst in different concentration of borohydride at 40 °C. Anode catalyst loading: 1 mg metal cm^{-2}, 0.5 ml min^{-1} × M $NaBH_4$ in 2 M NaOH. Cathode catalyst loading: 0.5 mg Pt cm^{-2}, dry O_2 at 0.1 l min^{-1} (2 atm).

Table 1
Cell performance for DBFC with various $NaBH_4$ concentrations.

Concentration of $NaBH_4$	0.2 M	0.5 M	1.0 M	1.5 M
Open circuit voltage (V)	1.051	1.049	1.015	1.013
Maximmn power density ($mW\,cm^{-2}$)	15	92	112	113
Maximum N_{app}	8	7.2	6.4	6.2

tently. On the B-AuPt/C catalyst in 0.2 M $NaBH_4$, the N_{app} value is approximate to 8, but the cell polarization performance is very low because the supply of fuel to the catalyst layer is inadequate. When the borohydride concentration increases from 0.5 to 1 M, the peak power density of the DBFC increases from 92 to 112 $mW\,cm^{-2}$. But it does not increase obviously for a further concentration increase. And the N_{app} value in 0.5 M is 7.2, decreasing to 6.2 in 1.5 M BH_4^-. The phenomenon is caused by the fact that the increasing BH_4^- concentration not only benefits the mass transfer and oxidation of the fuel, but also accelerates the BH_4^- hydrolysis. Therefore, choosing an appropriate $NaBH_4$ concentration to get a compromise between polarization performance and fuel efficiency is important.

4. Conclusions

The Pt-modified Au nanoparticles on carbon support, namely A-AuPt/C and B-AuPt/C, were prepared by the simultaneous and successive chemical reduction process respectively and compared with the unmodified Au nanoparticles. The Pt-modified Au nanoparticles (less than 5 nm in size) are highly dispersed on the carbon support. From analysis of CV and polarization curves of the DBFC, the B-AuPt/C catalyst shows the best anode catalytic activity when fed borohydride solution. The maximum power densities of the DBFC employing the B-AuPt/C, A-AuPt/C and Au/C catalysts are 112, 97 and 65 $mW\,cm^{-2}$, respectively. In addition, the DBFC employing B-AuPt/C as the anode catalyst shows the highest maximum fuel efficiency with N_{app} equal to 6.4 in 1 M $NaBH_4$ and N_{app} equal to 7.2 in 0.5 M $NaBH_4$. Thus the B-AuPt/C catalyst may serve as an efficient anode electro-catalyst for in a DBFC because of the high power output and fuel efficiency. Furthermore, the DBFC performance is influenced by the borohydride concentration and choosing an appropriate $NaBH_4$ concentration to get optimal polarization performance and fuel efficiency is also important.

References

[1] E. Gyenge, Electrochim. Acta 49 (2004) 965–978.
[2] J.H. Kim, H.S. Kim, Y.M. Kang, M.S. Song, S. Rajendran, S.C. Han, D.H. Jung, J.Y. Lee, J. Electrochem. Soc. 151 (2004) A1039–A1043.
[3] H. Dong, R.X. Feng, X.P. Ai, Y.L. Cao, H.X. Yang, C.S. Cha, J. Phys. Chem. B 109 (2005) 10896–10901.
[4] A. Verma, S. Basu, J. Power Sources 145 (2005) 282–285.
[5] M. Chatenet, F. Micoud, I. Roche, E. Chainet, Electrochim. Acta 51 (2006) 5459–5467.
[6] K. Deshmukh, K.S.V. Santhanam, J. Power Sources 159 (2006) 1084–1088.
[7] C. Ponce-de-León, D.V. Bavykin, F.C. Walsh, Electrochem. Commun. 8 (2006) 1655–1660.
[8] J.-H. Wee, J. Power Sources 155 (2006) 329–339.
[9] U.B. Demirci, J. Power Sources 172 (2007) 676–687.
[10] J.I. Martins, M.C. Nunes, R. Koch, L. Martins, M. Bazzaoui, Electrochim. Acta 52 (2007) 6443–6449.
[11] E. Sanli, B.Z. Uysal, M.L. Aksu, Int. J. Hydrogen Energy 33 (2008) 2097–2104.
[12] K. Wang, K. Jiang, J. Lu, L. Zhuang, C. Cha, X. Hu, G.Z. Chen, J. Power Sources 185 (2008) 892–894.
[13] K.T. Park, U.H. Jung, S.U. Jeong, S.H. Kim, J. Power Sources 162 (2006) 192–197.
[14] B.H. Liu, Z.P. Li, S. Suda, Electrochim. Acta 49 (2004) 3097–3105.
[15] S.M. Lee, J.H. Kim, H.H. Lee, P.S. Lee, J.Y. Lee, J. Electrochem. Soc. 149 (2002) A603–A606.
[16] Z.P. Li, B.H. Liu, K. Arai, S. Suda, J. Electrochem. Soc. 150 (2003) A868–A872.
[17] L. Wang, C. Ma, Y. Sun, S. Suda, J. Alloys Compd. 391 (2005) 318–322.
[18] Z. Yang, L. Wang, Y. Gao, X. Mao, C.-A. Ma, J. Power Sources 184 (2008) 260–264.
[19] M.H. Atwan, C.L.B. Macdonald, D.O. Northwood, E.L. Gyenge, J. Power Sources 158 (2006) 36–44.
[20] R. Jamard, A. Latour, J. Salomon, P. Capron, A. Martinent-Beaumont, J. Power Sources 176 (2008) 287–292.
[21] M.V. Mirkin, H. Yang, A.J. Bard, J. Electrochem. Soc. 139 (1992) 2212–2217.
[22] H. Cheng, K. Scott, Electrochim. Acta 51 (2006) 3429–3433.
[23] F.A. Coowar, G. Vitins, G.O. Mepsted, S.C. Waring, J.A. Horsfall, J. Power Sources 175 (2008) 317–324.
[24] P. Krishnan, T.-H. Yang, S.G. Advani, A.K. Prasad, J. Power Sources 182 (2008) 106–111.
[25] K. Wang, J. Lu, L. Zhuang, J. Phys. Chem. C 111 (2007) 7456–7462.
[26] I.-S. Park, K.-S. Lee, D.-S. Jung, H.-Y. Park, Y.-E. Sung, Electrochim. Acta 52 (2007) 5599–5605.
[27] X. Geng, H. Zhang, W. Ye, Y. Ma, H. Zhong, J. Power Sources 185 (2008) 627–632.
[28] M.M. Maye, N.N. Kariuki, J. Luo, L. Han, P. Njoki, L. Wang, Y. Lin, H.R. Naslund, C.-J. Zhong, Gold Bull. 37 (2004) 217.
[29] I.-S. Park, K.-S. Lee, Y.-H. Cho, H.-Y. Park, Y.-E. Sung, Catal. Today 132 (2008) 127–131.
[30] M. Chatenet, M.B. Molina-Concha, J.P. Diard, Electrochim. Acta 54 (2009) 1687–1693.
[31] Z.P. Li, B.H. Liu, J.K. Zhu, S. Suda, J. Power Sources 163 (2006) 555–559.
[32] Z.P. Li, B.H. Liu, K. Arai, K. Asaba, S. Suda, J. Power Sources 126 (2004) 28–33.
[33] B. Billyde, D.W. Scoot, R.S. Brian, T.G. Jeffrey, J. Electrochem. Soc. 155 (2008) B852–B859.
[34] A. Tegou, S. Armyanov, E. Valova, O. Steenhaut, A. Hubin, G. Kokkinidis, S. Sotiropoulos, J. Electroanal. Chem. 634 (2009) 104–110.